Inter-Laboratory testing for high temperature power generation characteristics of a Ni-based alloy thermoelectric module

Pawel Ziolkowski[a* †], Raju Chetty[b †], Przemyslaw Blaschkewitz[a], Michihiro Ohta[b], Atsushi Yamamoto[c*], Eckhard Müller[a,d]

[a]*German Aerospace Center (DLR) – Institute of Materials Research, Linder Höhe, D-51147 Cologne, Germany*

[b]*Global Zero Emission Research Center (GZR), National Institute of Advanced Industrial Science and Technology (AIST), Umezono 1-1-1, Tsukuba, Ibaraki 305-8568, Japan*

[c]*Research Institute for Energy Conservation, National Institute of Advanced Industrial Science and Technology (AIST), 1-1-1 Umezono, Tsukuba, Ibaraki 305-8568, Japan*

[d]*Institute of Inorganic and Analytical Chemistry, Justus Liebig University Gießen, Heinrich-Buff-Ring 17, D-35392 Gießen, Germany*

*Corresponding authors: Pawel Ziolkowski; Email: pawel.ziolkowski@dlr.de; Atsushi Yamamoto; Email: a.yamamoto@aist.go.jp

† These authors contributed equally to this work.

ORCID
PZ: 0000-0003-1519-6803
RC: 0000-0003-1072-8241
MO: 0000-0002-9093-7117
AY: 0000-0002-9210-2682
PB:
EM:

ABSTRACT

Standardization of metrology for thermoelectric generator modules (TEM) is a necessary step towards an industrialization of thermoelectric applications. Unspecified uncertainty budgets of the widely used custom built characterization facilities seem insufficient to validate technological developments, industrial benchmarks or allow sound conclusions in scientific studies. Particularly, works on high-temperature TEM have to be supported by suitable characterization techniques. This shall accelerate progress towards product releases for thermoelectric energy conversion. In this article we report on a Ni-based alloy TEM which was developed at the National Institute of Advanced Industrial Science and Technology (AIST) as a prospective standard reference TEM. Comparative measurements at AIST and the German Aerospace Center (DLR) demonstrate the high repeatability and precision of custom-built TEM characterization facilities at AIST and DLR. Tests at elevated temperatures up to 773 K hot side temperature and 450 K temperature difference revealed excellent accordance of electric measurands with a standard deviation < 0.3% for the open circuit voltage and < 0.85% for electric resistance and maximum power output. Deviations of the heat flow measurement of up to 7.22% arise from individual uncertainties of the employed characterization methods and point to the importance of standardization for TEM metrology.

Keywords: Thermoelectric Generator, Module, Standardization, Metrology, Uncertainty, Reference Module, Heat flow measurement, Reference Method, Absolute Method, Guarded Hot Plate, Rapid Steady State

1. INTRODUCTION

There is a lot of thermal energy wasted in terms of heat into the atmosphere day-to-day life. Recently, there has been paid much attention to the development of thermoelectric power generation technology, which can directly convert the wasted thermal energy into useful electrical power. This technology could play a crucial role in energy harvesting and limit the climate change through CO_2 reduction[1][2][3][4][5].

Thermoelectric generators (TEG) contain one or several thermoelectric generator modules (TEM) to convert heat into electric energy. A TEM is constructed from a variable number of thermocouples (p- and n-type legs) which are electrically connected in series by metallic bridges. A thermocouple operates under a temperature difference between a heat source and a heat sink and generates a thermovoltage at its terminals due to the Seebeck effect[6]. Beside mostly used planar types[7][8] TEM can be likewise constructed as cylindrical devices[9][10] in order to allow an easier installation on pipe-shaped heat reservoirs. A maximization of TEM performance can be achieved by application of functionally segmented[11][12] or graded[13][14] thermocouples or by application of cascaded[15][16] TEMs. The latter approaches target for the use of optimized materials with respect to a present temperature interval along the heat transmission path between a heat source and heat sink, which effectively allows for a better exploitation of the overall temperature differential and a maximization of the conversion efficiency. The efficiency η of a TEM is defined as the ratio between electric power output (P) and the incident heat flow at the hot side of a TEM (Q_{In}). Due to energy conservation, η can also be expressed as the ratio between P and the sum of P and Q_{Out} which is the released heat flow at the cold side of the TEM.

$$\eta = \frac{P}{Q_{In}} = \frac{P}{P + Q_{Out}} \tag{1}$$

As for any other heat engine the Carnot efficiency $\eta_C = (T_H - T_C)/T_H$, which is a function of the hot side temperature T_H and cold side temperature T_C, limits the maximum efficiency η_{MAX} of a TEM[17].

$$\eta_{MAX} = \frac{T_H - T_C}{T_H} \frac{\sqrt{1 + ZT_{avg}} - 1}{\sqrt{1 + ZT_{avg}} + \frac{T_C}{T_H}} \tag{2}$$

Practically, the physical properties of the thermoelectric materials together with further properties of the module affect η_{MAX} by the module's figure of merit ZT_{avg}. For a single TEM $ZT_{avg} = S^2/(R_i \cdot K) \cdot T_{avg}$ where S, K, R_i are effective values of the Seebeck coefficient, the thermal conductance, the electric resistance of the module, respectively, and T_{avg} as the mean temperature. Due to the interrelation of the temperature dependent material and system properties a maximization of the conversion efficiency requires usually comprehensive simulations in order to identify an optimized device design. Several works described appropriate methods and design tools to guide developers in this tasks[18][19][20][21][22][23][24]. Established Bi_2Te_3-based TEM can be ruled out for applications at elevated temperatures above 300 °C due to their limited temperature stability. The recent focus of international research on high temperature thermoelectric (TE) materials and contacting technologies for TEM integration resulted in the demonstration of various prototypes[25][26][27][28][29][30][31] and releases of small batch production by industries[32][33][34][35]. Decent technological maturity was shown for many thermoelectric material classes yielding TEM efficiencies of 8.9% for nanostructured half-Heusler module[36], 12% for segmented Bi_2Te_3/skutterudite module[37], 11% and 12% for segmented- and cascaded-Bi_2Te_3/nanostructured PbTe module, respectively[38][39].

Regardless of the type of characterization technique, the reliable specification of TEM efficiency remains still challenging due to missing guidelines for characterization protocols and standards of corresponding testing methods. Reference samples, which are still missing in the field of TEM metrology, represent a common and most effective way to set uncertainty budgets of widely used comparative measurement techniques.

In this work, we first introduce measurement facilities which are developed and operated at the German Aerospace Center (DLR) and the National Institute of Advanced Industrial Science and Technology (AIST), Japan. A Ni-based alloy module is introduced briefly, which was developed as a prospective standard reference sample[40]. Reference methods for the determination of heat flow are involved along with an absolute method to test this TEM. The suitability of the Ni-based alloy module as a reference for future metrological standard is demonstrated by the interlaboratory tests, which confirms the reproducibility and stability of thermoelectric power generation characteristics.

2. MODULE CHARACTERIZATION TECHNIQUES

TEM characterization covers determination of electric, thermal, and thermoelectric properties which have to be measured under variable installation and operation conditions. The two main approaches such as Harman method and steady state method have been used for the thermoelectric module characterization[41][42]. This article focusses on steady state methods only which involve a direct measurement of the heat flow by means of reference and absolute techniques.

After temperature stabilization the T_H and T_C can be measured either by a single or multiple temperature sensors placed in the direct vicinity of the TEM, or by an extrapolation from discretely localized temperature sensors in the direction of heat flow within the heat transfer blocks at both sides of the TEM. The open circuit voltage V_0 can be measured after temperature stabilization.

$$V_0 = N \cdot S_{\text{eff}} \cdot \Delta T = N \cdot S_{\text{eff}} \cdot (T_H - T_C) \quad (3)$$

The effective Seebeck coefficient S_{eff} can be calculated using N, the number of installed thermocouples within the TEM, and the temperature difference across the TEM $\Delta T = T_H - T_C$.

$$S_{\text{eff}} = \frac{V_0}{N \cdot (T_H - T_C)} \quad (4)$$

The heat flow $\dot{Q}$ can be calculated using the one-dimensional Fourier's law from the temperature difference ΔT_M within a heat flow meter (HFM)

$$\dot{Q} = -A_M \cdot \kappa_M \cdot \frac{\Delta T_M}{l_M} \quad (5)$$

with κ_M, A_M and l_M as the thermal conductivity, the cross sectional area and the length of the HFM section, which is equipped with temperature sensors. The heat flow can be measured alternatively by means of an absolute method. This technique is based on a guarded hot plate (GHP)[43][44][45][46] which is a metering heater surrounded by actively controlled guard heaters. The heat flow through the TEM is determined by measurement of the liberated Joule heat in the GHP which can be obtained from measurements of the electric current flow through the GHP I_{GHP} and the voltage drop V_{GHP}.

$$\dot{Q} = V_{GHP} \cdot I_{GHP} \tag{6}$$

The thermal conductance K of the TEM can be defined for open circuit conditions ($I = 0$) by the ratio between $Q = Q_{out} = Q_{in}\big|_{I=0}$ and ΔT. It has to be noted that K includes the contribution of the heat transfer coefficients between the TEM and the heat exchanging components within the measuring section.

$$K = \frac{\dot{Q}}{\Delta T} \tag{7}$$

The determination of further TEM properties requires an electric direct current (DC) flow through the TEM. This can be accomplished by means of an electronic load or passive resistor network, which has to be connected to the terminals of the TEM. Typically, the TEM current I is varied from zero up to the short circuit case. Due to the Peltier effect[47] every change of I alters the heat flow through the TEM, which requires a sufficient stabilization time to reach thermal steady state for successive measurements again.

The power output of the TEM P can be determined from concurrent measurements of I and the terminal voltage V.

$$P = V \cdot I \tag{8}$$

The maximum power output can be determined from a polynomial approximation of the obtained power parabola (Figure 1). Figure 1 shows exemplary characterization results, which were obtained on a prototype of a Skutterudite-based TEM from DLR. As the maximum power output is given for the condition of impedance matching ($R_i = R_{load}$) P_{Max} can be alternatively calculated from V_0^* and R_i.

$$P_{Max} = \frac{V_0^{*2}}{4 * R_i} \tag{9}$$

V_0^* denotes the open circuit voltage, which is obtained under the equilibrium temperature conditions for T_H and T_C at optimum current flow for a maximum power output. Finally, the efficiency can be calculated from results of heat flow and the power output by means of equation (1). The maximum efficiency can be determined from a polynomial approximation of the current dependent TEM efficiency.

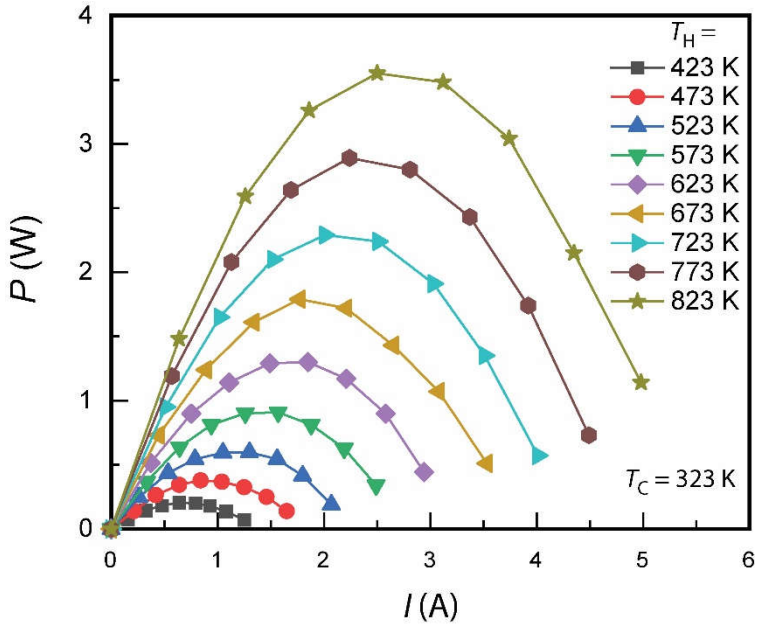

Figure 1: Measured power parabola curves of a high temperature TEM, which was tested at a constant T_C = 323 K and various hot side temperatures T_H between 423 K and 823 K. The temperatures relate to open circuit conditions.

3 THERMOELCTRIC MODULE CHRACTERIZATION FACILITIES AT AIST AND DLR

3.1 REFERENCE METHOD FOR HEAT FLOW DETERMINATION (AIST and DLR)

This section gives a brief survey on the custom-made TEM characterization facilities at AIST[25][48] (Figure 2a) and DLR (Figure 2b)[49] with respect to the applied techniques, construction of measuring sections, specific differences in the instrumentation and evaluation procedures which are relevant for the uncertainty of particular measurands.

Both facilities use oxygen-free copper heat exchangers and HFM with high thermal conductivity in order to improve the temperature homogeneity on the coupling faces at the hot and cold side of the TEM. After installation of the TEM, measuring sections at DLR are thermally dammed in order to decrease lateral heat losses, which impair the one-dimensionality of the heat flow and consequently the accuracy of measurements. However, at AIST the Ni-based alloy TEM is not thermally insulated, which is expected to have some influence on the heat flow (discussed in section 5.1). Figure 2c and Figure 2d shows the assemblies of the measuring sections and in case of Figure 2d prior to thermal damming.

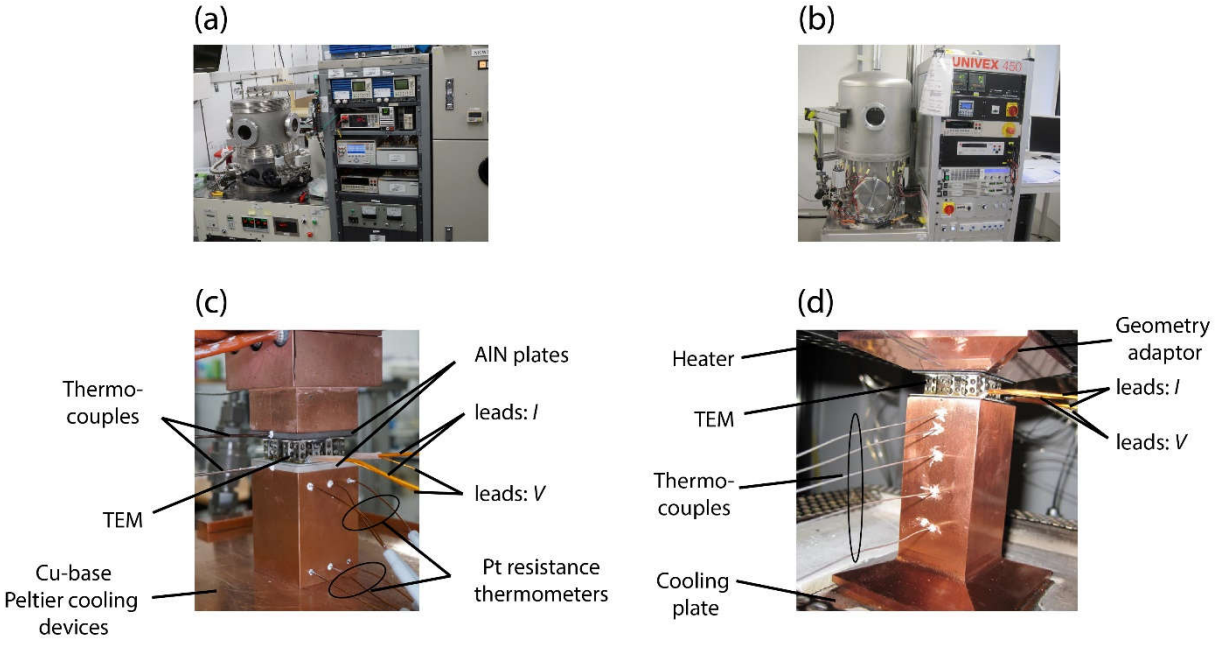

Figure 2: TEM characterization facilities at AIST (a) and DLR (b). Measuring sections at AIST (c) and DLR (d) facilities with reference heat flow determination.

At AIST, a HFM with same cross section of the TEM was used at the cold side of the TEM, whereas a Cu block with same cross section was applied at the hot TEM side for thermal coupling towards the heater. Six Pt resistor thermometers with 1.05 mm diameter were placed in two horizontal layers at a vertical distance of 40 mm to measure the temperature drop ΔT_M along the cold side HFM. The temperatures T_H and T_C at the TEM are measured and controlled by two thermocouples (Type K, 1.05 mm diameter). These sensors are embedded within two AlN plates (30 x 30 x 2 mm³), which are in direct contact on both sides of the TEM. A graphite foil (0.127 mm thick, Grafoil®) was used for thermal coupling between the hot-side Cu block and the AlN ceramic plate as well as between this AlN ceramic plate and the hot side of the module. Thermal grease (KS-613, ShinEtsu Silicone) was used for thermal coupling between the cold side of the module and the AlN ceramic plate as well as between this AlN ceramic plate and the cold side Cu HFM.

At DLR, a HFM was used at the cold side of the TEM with same cross section of the TEM. The hot side of the TEM is coupled to the heater by a truncated pyramid which has a height of 14 mm and a cross section of 30 x 30 mm² (TEM side) and 65 x 65 mm² (heater side), respectively. Three type-N thermocouples (0.5 mm diameter, Inconel sheath, 1NI05/1000/MP/FM.N, Thermo Expert) are placed with a vertical distance of 2 mm within the pyramid to determine T_H from an extrapolation towards the TEM coupling face. Similarly, in order to determine T_C at the cold side of the TEM by extrapolation from the cold side HFM, five thermocouples (same type as used within the pyramid) are placed with a gradually decreasing vertical distance between 15 mm and 5 mm in the direction towards the TEM. These sensors are used also to measure the temperature drop ΔT_M along the cold side HFM for determination of the released heat flow at the cold side of the TEM. A 0.2 mm thick graphite foil (Dr. Fritsch Sondermaschinen GmbH) is used for thermal coupling between all parts of the measuring section (heater, pyramid, TEM, heat flow meter, cooling plate).

The error of the heat flow determination at AIST is estimated with ±3%. The error in the heat flow measurement is mainly due to the 2.5% uncertainty in the thermal conductivity of Cu block, which is calibrated using Standard Reference Materials of the National Institute of Standards and Technology (NIST SRM) pure electrolytic iron and partially due to the uncertainty in the temperature measured by Pt resistance thermometers [40]. The uncertainty of the reference method at DLR was determined from repetitive measurements[49] on a certified thermal reference material from the National Physical Laboratory (Inconel 600, NPL 2I09)[50], which yielded the derivation of the full uncertainty budget. The uncertainty of the heat flow measurement was determined in accordance to the "*Guide to the expression of uncertainty in measurement*" (GUM)[51]. The maximum combined uncertainty $u(Q)$ equals ±6.5% (k = 1) within the temperature range between 423 K and 823 K. The coverage probability, which is expressed by the coverage factor k, equals 68.27% in this case (for k = 1). A coverage probability of 95% is reached for k = 2, yielding $u(Q)$ = ±13% (k = 2).

3.2 ABSOLUTE METHOD FOR HEAT FLOW DETERMINATION (DLR)

At DLR, absolute heat flow determination is based on a guarded hot plate (GHP). The GHP is a metering heater, which effectively transfers the measurement of the heat flow into an electric measurement of the consumed electrical power which is dissipated inside the heater as Joule heat. The metering heater is surrounded by guard heaters in order to establish ideally isothermal conditions to prevent side heat losses. The real conditions deviate from this ideal situation due to internal temperature gradients along the heat transmission path between the GHP and the TEM. This temperature gradient is a result of the heat flow, which is generated by the GHP, and the finite thermal conductivity of the used materials for heat transmission. The GHP is operated in a custom-made facility at DLR. Technically this facility is a duplicate of the facility described above except the GHP, its power supplies and PID multichannel temperature controllers. Figure 3 shows the GHP-based facility with the heater construction on top of the measuring section.

Figure 3: Facility at DLR for the characterization of TEM by means of an absolute method for heat flow determination (a). View into the measuring chamber with measuring section (b), with the thermal damming enclosing the measuring section being dismounted.

A thick film pyrolytic graphite heater enclosed in a boron nitride encapsulation (Boralectric®, TECTRA) is used as the GHP core element, the metering heater. The GHP is embedded within a Cu shell, for homogenization of temperature and heat flow. The lower surface of the shell is used for thermal coupling with the TEM sample or with the measuring section (Figure 4).

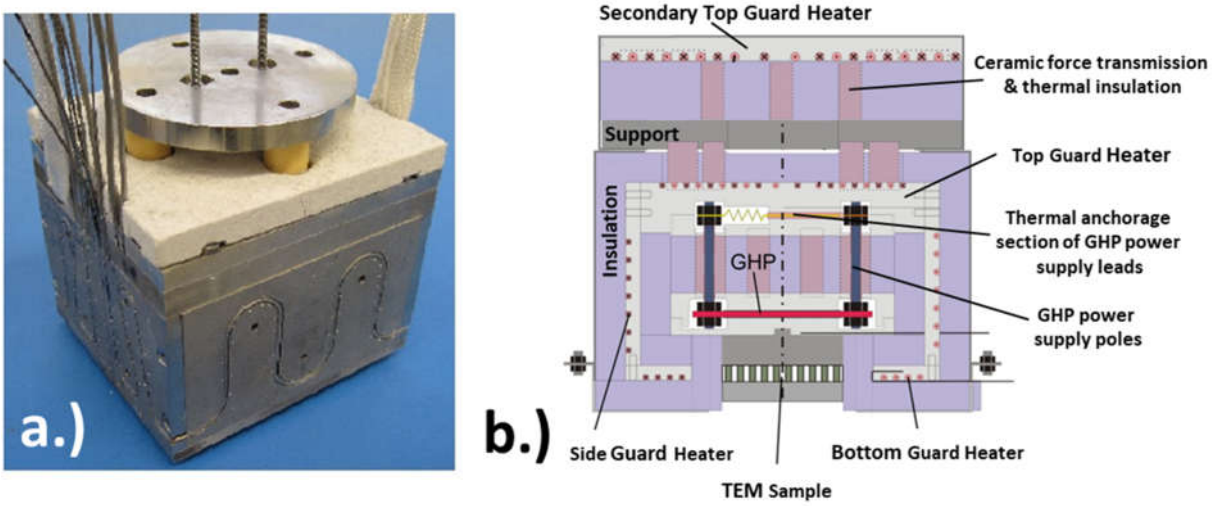

Figure 4: Absolute heater system with upper support plate, without outer insulation (a) and corresponding schematic (b) showing the basic arrangement of the GHP, guard heaters, and passive insulation components.

Investigations on the accuracy of the GHP-based heat flow determination were carried out using a certified thermal reference material (NPL 2109, Inconel600)[49]. The comparison to reference values in the temperature range between 423 K and 823 K revealed a deviation of the heat flow determination by the GHP of $u(Q) < \pm 2.41\%$ ($k = 2$). This deviation is lower than the specified uncertainty of the thermal reference material which equals $u(\kappa) = \pm 4.8\%$ ($k = 2$). Hence this uncertainty specification for the GHP is not meaningful. In order to determine the GHP uncertainty more reliably, the effective cross talk between the GHP and the guard heaters was determined by thermal detuning experiments. The data analysis yielded a resulting uncertainty of the heat flow determination by the GHP of $u(Q) < \pm 0.75\%$ ($k = 2$) in the temperature range between 423 K and 823 K.

3.3 EVALUATION OF INTERNAL ELECTRICAL RESISTANCE

For both facilities at AIST and DLR, the TEM is connected to the electric measurement circuit in a four point scheme. Two leads are connected to the terminals of the TEM to conduct *I*. Close to this connection points two additional sensor cables are used to measure the terminal voltage *V*. This prevents the impact of electric contact resistances between the supplying leads and the TEM terminals on the measurement of *V*.

Rapid Steady State (RSS) method (DLR)

Evaluating the slope of the *I*-*V* characteristic (black curve in Figure 5) gives access to the internal electric resistance R_i of a TEM. Figure 5 shows an exemplary *I*-*V* characteristic, which shall emphasize the appearance of such measurement curves only. These results have been obtained in DLR facility on the same prototype of a Skutterudite-based TEM, which was already introduced for the presentation of the typical appearance of the power parabola (Figure 1).

$$R_i^{SS} = \frac{V_1 - V_2}{I_1 - I_2} \tag{10}$$

However, the simple derivation d*V*/d*I* according to equation (10) under steady state (SS) conditions leads to an overestimation of R_i, due to a decreasing open circuit voltage V_0*, which is caused by the Peltier-induced reduction of the effective temperature difference ΔT across the TEM in presence of a direct current flow as a result of the limited thermal conductance of the heat transfer blocks when the heater and cooler temperatures are stabilized. This effect on a DC-based measurement of R_i is mitigated in two ways at DLR. First, the original temperature difference (at $I = 0$) can be restored under current flow by adjustment of the temperature set points of the heater and the cooling device. This procedure needs additional stabilization time in order to reach thermal steady state conditions within the measuring section. Alternatively, the decreasing level of V_0* can be measured by a fast signal sampling during the switching event of *I* ($I \rightarrow 0$). This technique is similar to the method, which was used by McCarty et al.[52] and Mahajan et al.[53], who has called this approach earlier as the rapid steady state (RSS) method. After thermal stabilization under a constant *I*, the TEM circuit is opened. Analog to the Harman method for determination of ZT_{avg}[41][42], immediately after the switching event the response of the terminal voltage consists of an instantaneous step function due to the ceasing Ohmic voltage drop and a transient component, which is determined by the thermal relaxation process of the effective temperature difference. V_0* is measured by means of a fast signal sampling (2 kHz sampling frequency) of the terminal voltage *V* during the switching event, which is repeated up to ten times in order to increase the accuracy by a static evaluation of the obtained voltage values.. Determination of V_0* allows for a Peltier-corrected value of R_i^{RSS}, which can be calculated from measurements of ΔV_1, ΔV_2, and the corresponding current values I_1 and I_2, respectively (Figure 5).

$$\begin{aligned} \Delta V_1 &= V|_{I_1 \rightarrow 0} - V|_{I = I_1} \\ \Delta V_2 &= V|_{I_2 \rightarrow 0} - V|_{I = I_2} \\ R_i^{RSS} &= \frac{\Delta V_1 - \Delta V_2}{I_1 - I_2} \end{aligned} \tag{11}$$

Alternatively, the internal electric resistance can be measured likewise by application of a small alternating current (AC) signal and an evaluation using equation (10). The choice of a sufficiently high

frequency for the AC current excitation avoids the impact of the Peltier effect but requires additional measurement instrumentation, such as Lock-In amplifiers for the separation of the real part and the reactance of the measured impedance.

AC resistance measurement (AIST)

At AIST, AC resistance is measured by an inductance–capacitance–resistance (LCR) meter [48]. The frequency of the signal is 1 kHz, but this AC signal does not affect the measurement of the power generation characteristics, which are DC phenomena. It should be noted that the AC resistance measured directly by the LCR meter is not the same as the resistance determined from the *I-V* characteristics of the module. The DC resistance, calculated as the slope of the *I*–*V* plot, inevitably includes the Peltier effect, meaning that the DC resistance is always larger than the AC resistance, the latter avoiding the Peltier effect.

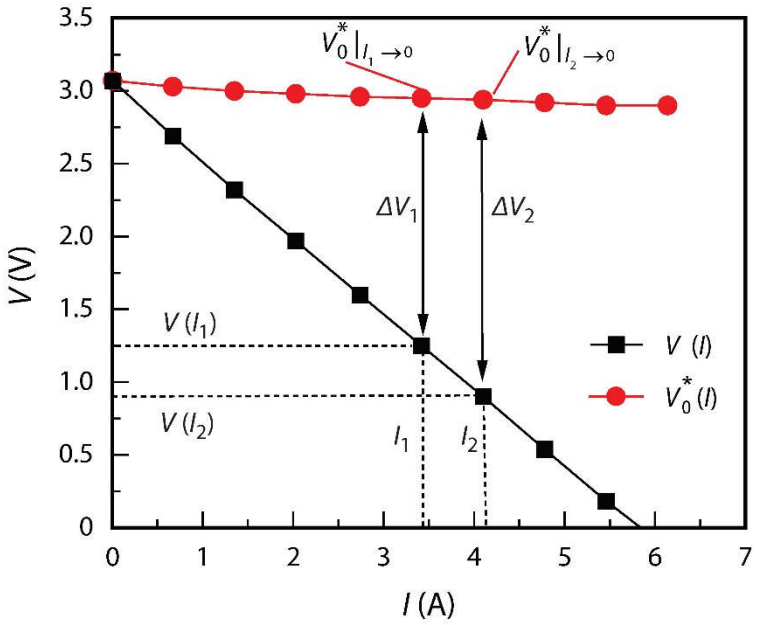

Figure 5: The *I-V* curve measured in DLR facility shows the TEM terminal voltage *V* in dependence of the current flow *I* (black curve) at fixed heater and cooler temperature. The Peltier effect causes a decreasing open circuit voltage V_0* (red curve) with increasing current flow as a result of the limited thermal conductance of the heat transfer blocks in series to the TEM (see Fig. 2).

4 NI-BASED REFERENCE MODULE

The use of p-type $Ni_{90}Cr_{10}$ (chromel) and n-type $Cu_{55}Ni_{45}$ (constantan) thermoelectric elements in TEM (Figure 6) for metrological purposes offers the advantage of an easy contacting and promises better functional and mechanical stability for the TEM. In order to increase the electric and thermal resistance of the legs, four holes with a diameter of 2 mm were drilled into every element, yielding a reduction of the effective density to 57.1%. The TEM was built from 8 pairs of p- and n-type legs on a Si_3Ni_4 substrate with dimensions of 28 mm x 28 mm x 0.32 mm. The integral thermal resistance of the Ni-based TEM equals R_{th} = 6.16 KW^{-1} [40] which matches with the value of usually tested samples. Thus, the heat flux at a certain temperature difference will fit to the appropriate interval in order to derive meaningful values for the accuracy of the applied testing method. Further

information on the Ni-based TEM including a comparison of measurement results obtained on two prototypes (with and without drilled holes within their legs) and corresponding FEM-simulations are reported in [40]. Note that a comparison of FEM simulations (without consideration of radiative heat transport inside the leg holes) and a measurement at T_H = 773 K revealed a heat flow difference of only 2 W (simulated: 71 W, measured 73 W)[40], which gives rise to the assumption that only a relative contribution of 1.46% of the overall heat flow is provided by radiation inside the holes.

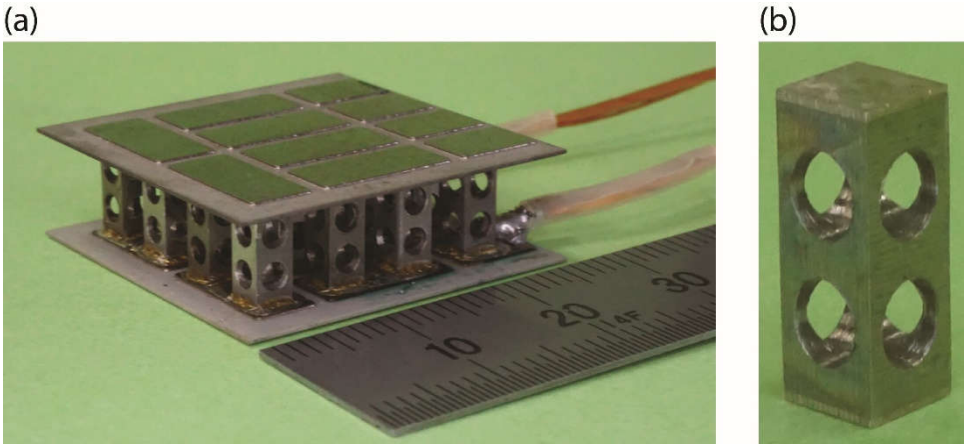

Figure 6: Prototype of the Ni-based alloy thermoelectric generator module (a) and a single thermoelectric element (b).

A comparison of other thermoelectric properties of the used Ni-based alloys with those of usually applied TE materials within TEMs shows significant differences for the electric conductivity and the Seebeck coefficient, too. While the internal electric resistance is shifted to a representative level of a few tens of mΩ by the drilled leg holes (Figure 8), the Seebeck coefficient is not sensitive to any changes of the leg geometry. Consequently a reduced Seebeck coefficient will cause a measurement of lower thermovoltages, electric power output, and TEM efficiency, too. The corresponding effects on the reliability of future device calibrations by means of measurements on the Ni-based alloy TEM shall be discussed briefly at this point.

Generally, lower thermovoltages put higher requirements on the accuracy of the involved measurement instrumentation and the control of temperature differentials as the driving force for the generation of thermovoltages. If a low deviation is recognized for the low level of the specified thermovoltage of the Ni-based alloy TEM one can assume equal or even reduced uncertainty contributions during characterization of TEMs with high performance TE materials, which possess higher Seebeck coefficients and consequently generate higher thermovoltages. Consequently any observed measurement deviation in comparison to specified thermovoltage values of the Ni-based alloy TEM can be recognized as an upper uncertainty limit in first approximation. This is likewise true for the measurement of the electric power output, since the low thermovoltage of the Ni-based alloy TEM yields inevitably a significantly lowered current range, too. Any observed deviations for the low power output and the correspondingly low level of efficiency of the Ni-based alloy TEM represent upper limits for uncertainties during characterization of TEMs with better thermoelectric properties.

Due to the significantly lowered Seebeck coefficient special regard has to be paid to the impact of the reduced Peltier heat transport through the Ni-based alloy TEM. The lower the level of Peltier heat the lower the detuning of V_0* becomes in the course of variations of the electric current flow through a TEM (see section 3.3). Since the change of V_0* can be recognized as the fingerprint of the reduced temperature difference over the TEM, characterization of samples with better TE properties

might be exposed to an increased level of temperature detuning compared to calibration experiments with the use of the Ni-based alloy TEM. However, this still gives no rise to an insignificance of the underlying uncertainty for measurands like the internal electric resistance, power output and efficiency of high performant TEMs. If the significantly smaller temperature detuning and changes of V_0* are correctly measured on the Ni-based alloy TEM, users can assume similar or even lower uncertainties during characterization of high performant TEM, too.

5. MEASUREMENT RESULTS

After tests at AIST[40] the TEM was send to DLR for characterization. Two measurements with intermediate re-installation of the TEM were performed at DLR (M04, M05) in order to compare with results from M01. Table 1 gives a survey of conducted measurements.

Table 1: Measurements on a Ni-based alloy TEM listed in chronological order. Thermal boundary conditions of every measurement are given, as well as information on intermediate re-installations of the TEM, used facilities, duration of stability tests, and the general purpose of each measurement.

Measurement	Temperature Conditions [K]	Remarks / Reference
M01 – AIST	T_C = 323 / T_H = 473, 573, 673, 773	Initial full characterization (Figure S1) / [40]
M02 – AIST	T_C = 323 / T_H = 773	Reproducibility study: 12 measurements with TEM re-installation / [40]
M03 – AIST	T_C = 323 / T_H = 773	Stability study: 120 h total duration, Intermediate measurements after 5h / [40]
M04 – DLR	T_C = 323 / T_H = 473, 573, 673, 773	Electric characterization: After shipping
M05 – DLR	T_C = 323 / T_H = 473, 573, 673, 773	Full characterization (Figure S1): TEM re-installed, absolute and reference heat flow measurement

5.1 COMPARATIVE MEASUREMENTS AT AIST AND DLR

The data comparison between M01 (AIST) and M04 and M05 (DLR), respectively, allowed for a further verification of the module stability and a methodical assessment on similarities and differences of the measurement facilities and evaluation procedures. Despite individual means for thermal coupling of the TEM at AIST and DLR an excellent accordance of the open circuit voltage V_0 could be observed (Figure 7). The resulting standard deviation $\sigma(V_0)$ remained below ~0.3% over the entire temperature range. This agreement is a strong argument for almost identical temperature conditions at the thermoelectric elements during all measurements. This indicates a high temperature homogeneity and equality of thermal transfer resistances at the TEM coupling, which reflects a high accuracy and comparability of the control of thermal and mechanical installation conditions. Secondly, the observed accordance indicates stable thermal transfer resistances between the Si_3Ni_4 substrate, the metallic bridges and the thermoelectric elements, which is in fact a proof of

the internal TEM contact quality and stability. Due to the dependence of V_0 on S_{eff}, the repeatability and accordance of V_0 data supports the conclusion of stable thermoelectric properties of the Ni-based alloys under the tested conditions, too.

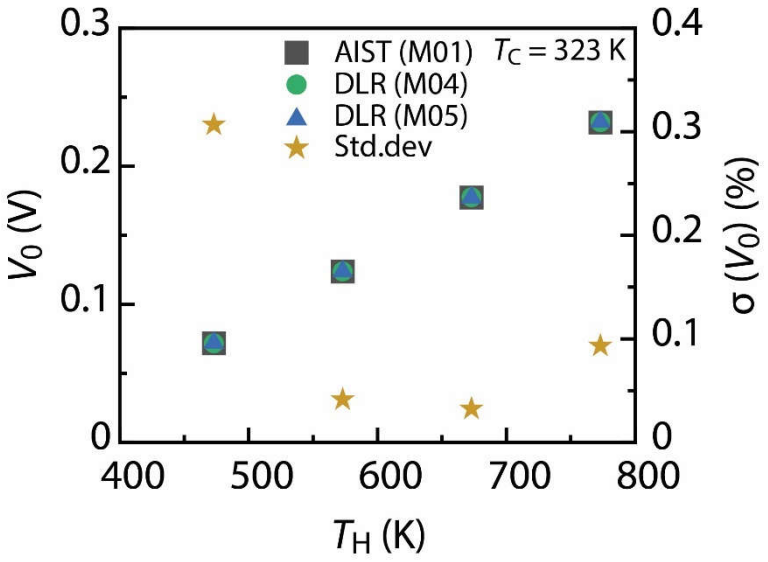

Figure 7: Comparison of the open circuit voltage V_0 in dependence of the hot side temperature T_H, measured at AIST (M01) and DLR (M04, M05). The relative standard deviation $\sigma(V_0)$ was calculated for the temperature dependent mean value under consideration of all conducted measurements.

R_i was determined at AIST from an evaluation of the steady state *I-V* characteristics and secondly from an AC-based measurement by means of a small signal excitation. A comparison of these results (Figure 8a) confirms the overestimation of R_i from a direct evaluation of the *I-V* characteristic obtained under steady state conditions of a DC-based measurement on a TEM. This was described in [47] by an analytic expression for V_0* as a function of *I* and the conductances of a dissipative coupling between the TEM and the heat baths. In contrast, AC-based resistance measurements cannot be influenced by the Peltier effect, if a sufficiently high frequency (1 kHz) is chosen. The corresponding results reflect a mean deviation of ~8% between the DC- and AC-based measurements of R_i at AIST. It is worth to note, that the deviation stems from a reduced open circuit voltage due to a decreasing temperature difference in presence of a current-induced Peltier heat transport. The transported Peltier heat is directly proportional to the current flow and the effective Seebeck coefficient, which is considerably low for the Ni-based alloy TEM and equals S_{eff} ~ 66 µV K^{-1} for a single thermocouple at a temperature difference of 450 K. Thus, the resulting deviation between DC- and AC-based measurements might even exceed 8% for TEM, which are built from typically applied high temperature TE materials, due to their higher S_{eff}. DLR results on R_i are based on the RSS method, which reduces the impact of the Peltier effect. However, a calculation of the mean value from DLR and AC-based AIST results shows a moderate standard deviation $0.45\% < \sigma(R_i) < 0.85\%$ within the tested temperature range (Figure 8b). In view of the low value of $\sigma(V_0)$ the higher value of $\sigma(R_i)$ cannot stem from deviating temperature conditions only. One reason might be an under-correction of the Peltier impact by the applied RSS method at DLR due to a too slow signal sampling and related uncertainties of the determination of V_0*. This assumption is indicated by the monotonous increase of $\sigma(R_i)$ with increasing T_H, which coincides with the increase of S_{eff} and the thermal conductivity of the Ni-based alloys[40] . While the first yields an increase of the Peltier heat transport in general, the latter reduces the time constant of the thermal relaxation after switch-off of the electric current. However, considering the typical uncertainties of electric

measurements of the terminal voltage and the current flow through a TEM, the observed level for $\sigma(R_i)$ can be still considered as an acceptable low value.

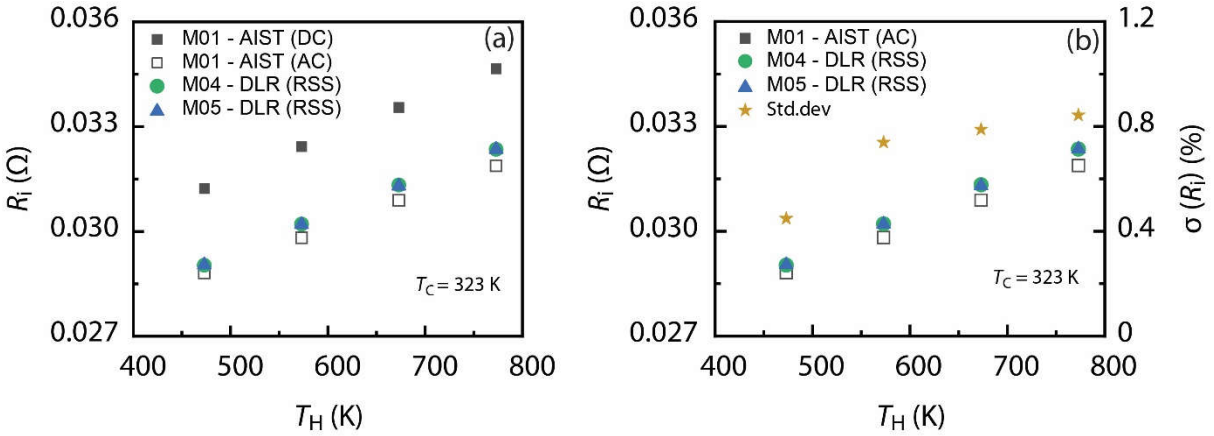

Figure 8: Comparison of the internal electric resistance R_i in dependence of the hot side temperature T_H (a), measured at AIST (M01) and DLR (M04, M05). Results from AIST are based on an evaluation of the steady state *I-V* characteristic (DC – full black symbols) and data from an AC-based measurement (AC – blank black symbols). DLR results were obtained by means of the rapid steady state (RSS) method. The relative standard deviation $\sigma(R_i)$ was calculated for the temperature dependent mean value leaving data from the DC measurement out of consideration (b).

Comparison of P_{Max} values measured at AIST and DLR is shown in Figure 9a. The mean deviation for P_{Max} equals 7.9% for DC- and AC-based measurements at AIST, which corresponds to the difference of measured R_i values. Neglecting again the DC-based evaluation of P_{Max} yields a reasonably low deviation to the outcome at DLR. The resulting standard deviation of the mean value was $0.65 < \sigma(P_{Max}) < 0.81\%$ (Figure 9b).

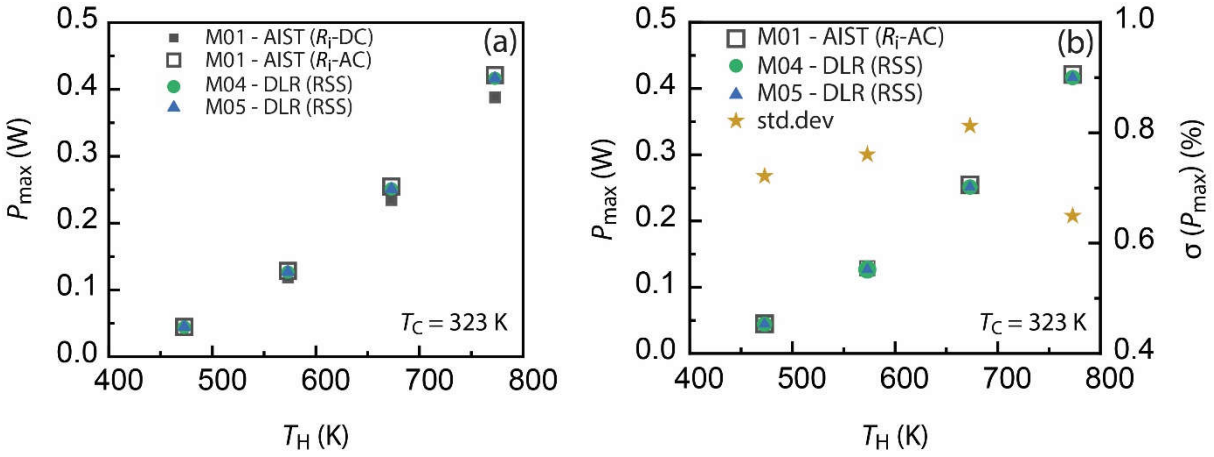

Figure 9: Comparison of the maximum power output P_{Max} in dependence on the hot side temperature T_H (a), measured at AIST (M01) and DLR (M04, M05). Results from AIST are based on an evaluation of the *I-V* characteristic under consideration of R_i from a DC-based steady state measurement (R_i – DC / full black symbols) and an AC-based measurement (R_i – AC / open black symbols). DLR results were obtained from a fit of the power parabola $P(I)$. The relative standard deviation $\sigma(P_{Max})$ was calculated for the temperature dependent mean value (b) disregarding DC-based steady state measurement of R_i.

The highest deviation between the employed characterization methods was observed for the measurement of the heat flow. The standard deviation showed a monotonous increase with T_H and amounted to $3.73\% < \sigma(Q_{Out}) < 7.22\%$ (Figure 10a). The error bars in this figure correspond to the previously discussed uncertainties for heat flow determination of the respective characterization facilities. The uncertainties of the applied reference methods at AIST and DLR yield a hardly

overlapping confidence interval. As mentioned in section 3.1 that the TEM is thermally insulated to avoid the lateral heat losses during the heat flow measurement at DLR, whereas it is not in case of heat flow measurement at AIST. Therefore, radiation losses could be a possible reason for the discrepancy in the heat flow between AIST and DLR measurements. This is supported by the monotonous increase of deviation with increasing hot side temperature, since radiative heat transfer increases steadily as temperatures rise. A precise quantification of radiation losses and specification of resulting uncertainty contributions to the measurement of heat flow is not possible at the moment due to the lack of corresponding data. Future investigations have to be conducted on the radiation transport along the measuring sections in order to determine this elusive and parasitic effect on the heat flow measurement. However, note that the measurement data obtained at DLR by means of the reference and absolute method showed a reasonable accordance with a mean deviation of 1.5% over the entire temperature range, which reflects a general suitability to perform accurate measurements by means of both methods. The standard deviation of the maximum efficiency is mainly resulted from the deviation of Q_{out}, leading to the values of 3.6% < $\sigma(\eta_{Max})$ < 8.1% (Figure 10b).

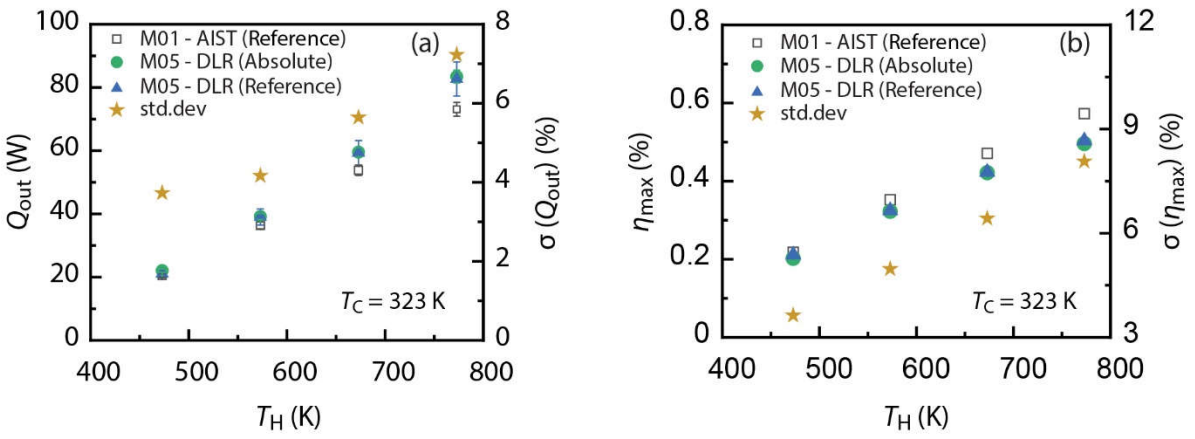

Figure 10: Comparison of the outgoing heat flow Q_{Out} (a) at maximum efficiency condition and the maximum efficiency η_{Max} (b) in dependence of the hot side temperature T_H, measured at AIST (M01) and DLR (M05). Results from DLR show data obtained from the reference and absolute (GHP) method for heat flow determination. The relative standard deviations $\sigma(Q_{Out})$ and $\sigma(\eta_{Max})$ were calculated for the temperature dependent mean values under consideration of all data.

6. CONCLUSION

A Ni-based alloy TEM, which was produced at AIST as a prospective reference sample for TEM metrology, was tested at AIST and DLR. The measurements were performed under nominally identical thermal and mechanical installation conditions but different media for thermal coupling of the TEM to the measuring head. Data comparison revealed excellent accordance of electric properties within the tested hot side temperature range of 473 K < T_H < 773 K. The standard deviation of the open circuit voltage was within 0.3%, while for the electric resistance and the maximum power output the standard deviation did not exceed a value of 0.85%. The highest deviation was observed for the heat flow which reflects the continuing demand on standardization for TEM metrology. Comparison of a reference and an absolute measurement technique of heat flow measured at DLR revealed a reasonable deviation of 1.5%. Comparison between the reference method used at AIST and the outcome at DLR gave a maximum standard deviation of 7.22%. According to the requirements on the qualification of reference samples[54], additional

measurements are necessary to give proof of the batch homogeneity (repeatability of module properties) and the long and short time stability under application conditions. Furthermore thorough uncertainty analyses have to be provided in future for all measurands, too, in order to enable a distinction between metrological uncertainty contributions of the employed measurement facilities and possible changes on sample properties in the course long term stability investigations. Beforehand, the Ni-based alloy TEM gives a good possibility for a preliminary verification of measurement uncertainties and for the conduct of comparative measurement campaigns. This may pave the way for thermoelectric standardization in order to increase the confidence level of TEM metrology.

Author contributions

Conceptualization, P.Z., E.M, M.O, A.Y.; Data analysis & writing-original draft, P.Z., P.B., R.C., M.O., A.Y.; Writing–Review & Editing, all authors, Funding Acquisition, P.Z., A.Y., M.O.

Conflicts of interests

M.O. and A.Y. are cofounders of Mottainai Energy Co., Ltd. M.O. is also its technical adviser. Mottainai Energy Co., Ltd. does not fund the work or participate in its execution**.**

7. ACKNOWLEDGEMENTS

This work was accomplished in the course of the project “Thermoelectric Standardization for High Temperatures” (TEST-HT, grant number 03VP04401), which was supported by the German Federal Ministry of Education and Research. Further financial support from the Energy Efficiency & Resource Core Technology Program of the Korea Institute of Energy Technology Evaluation and Planning (KETEP) was granted from the Ministry of Trade, Industry & Energy (MOTIE), Republic of Korea (no. 20188550000290). This work was supported by the International Joint Research Program for Innovative Energy Technology funded by the Ministry of Economy, Trade and Industry (METI), the Research and Development Project for Innovative Thermal Management Materials and Technologies funded by Thermal Management Materials and Technology Research Association (TherMAT) and New Energy and Industrial Technology Development Organization (NEDO), and Research and Development Program for Promoting Innovative Clean Energy Technologies Through International Collaboration funded by NEDO. We thank Mr. Kazuo Nagase for the fabrication of Ni-based alloy module and Mr. Hiroyuki Takazawa for the module testing.

8. REFERENCES

[1] L. E. Bell, *Science,* **2008**, *321*, 1457.

[2] G. J. Snyder, In *Energy Harvesting Technologies*; Shashank Priya; Inman, D. J., Eds.; Springer US: Boston, MA, 2009; pp. 325–326.

[3] D. M. Rowe, In *Thermoelectrics and its Energy Harvesting: Modules, Systems, and Applications in Thermoelectrics*; Rowe, D. M., Ed.; CRC Press: Boca Raton, 2012; pp. 23–1–23–21.

[4] J. Yang, F.R. Stabler, In *Thermoelectrics and its Energy Harvesting: Modules, Systems, and Applications in Thermoelectrics*; Rowe, D. M., Ed.; CRC Press: Boca Raton, 2012; pp. 25–1–25–15.

[5] D. Enescu, In *Green Energy Advances*; Enescu, D., Ed.; IntechOpen, 2019; Vol. i, pp. 1–37.

[6] D. M. Rowe, In *Thermoelectric Handbook - Macro to Nano*; Rowe, D. M., Ed.; Taylor & Francis Group: Boca Raton, 2006; pp. 1–1.

[7] P. Markowski, A. Dziedzic, *Microelectron. Reliab.* **2008**, *48*, 890.

[8] N. Jaziri, A. Boughamoura, J. Müller, B. Mezghani, F. Tounsi, M. Ismail, *Energy Reports* **2019**.

[9] A. Schmitz, C. Stiewe, E. Müller, *J. Electron. Mater.* **2013**, *42*, 1702.

[10] H. Jang, J. B. Kim, A. Stanley, S. Lee, Y. Kim, S. H. Park, M.-W. Oh, *Energies* **2020**, *13*, 1106.

[11] R. A. Kishore, M. Sanghadasa, S. Priya, *Sci. Rep.* **2017**, *7*, 16746.

[12] H. Tian, N. Jiang, Q. Jia, X. Sun, G. Shu, X. Liang, *Energy Procedia* **2015**, *75*, 590.

[13] E. Müller, K. Zabrocki, C. Goupil, G. J. Snyder, W. Seifert, In *Materials, Preparation, and Characterization in Thermoelectrics*; CRC Press, 2017; pp. 46–81.

[14] C. L. Cramer, H. Wang, K. Ma, *J. Electron. Mater.* **2018**, *47*, 5122.

[15] H. T. Kaibe, L. Rauscher, S. Fujimoto, T. Kurosawa, T. Kanda, M. Mukoujima, I. Aoyama, H. Ishimabushi, K. Ishida, S. Sano, *Proc. 23rd Int. Conf. Thermoelectr.* **2004**.

[16] H. Zhang, W. Kong, F. Dong, H. Xu, B. Chen, M. Ni, *Energy Convers. Manag.* **2017**, *148*, 1382.

[17] A. F. Ioffe, L. S. Stil'bans, E. K. Iordanishvili, T. S. Stavitskaya, A. Gelbtuch, G. Vineyard, *Phys. Today* **1959**, *12*, 42.

[18] M. Hong, K. Zheng, W. Lyv, M. Li, X. Qu, Q. Sun, S. Xu, J. Zou, Z.-G. Chen, *Energy Environ. Sci.* **2020**, *13*, 1856.

[19] M. Hong, W. Lyu, Y. Wang, J. Zou, Z.-G. Chen, *J. Am. Chem. Soc.* **2020**, *142*, 2672.

[20] B. Ryu, J. Chung, S. Park, *Thermoelectric efficiency has three Degrees of Freedom*; 2018.

[21] B. Ryu, J. Chung, E.-A. Choi, P. Ziolkowski, E. Müller, S. Park, *Appl. Phys. Lett.* **2020**, *116*, 193903.

[22] P. Ponnusamy, J. de Boor, E. Müller, *Appl. Energy* **2020**, *262*, 114587.

[23] P. Ponnusamy, J. de Boor, E. Müller, In *International Conference on Thermoelectrics (ICT)*; 2019.

[24] K. Zabrocki, E. Mueller, In *International Conference on Thermoelectrics (ICT)/European Conference on Thermoelectrics (ICT) 2015, At Dresden, Germany*; 2015.

[25] J. R. Salvador, J. Y. Cho, Z. Ye, J. E. Moczygemba, A. J. Thompson, J. W. Sharp, J. D. König, R. Maloney, T. Thompson, J. Sakamoto, H. Wang, A. A. Wereszczak, G. P. Meisner, *J. Electron. Mater.* **2013**, *42*, 1389.

[26] J. García-Cañadas, A. V. Powell, A. Kaltzoglou, P. Vaqueiro, G. Min, *J. Electron. Mater.* **2013**, *42*, 1369.

[27] T. Ochi, G. Nie, S. Suzuki, M. Kikuchi, S. Ito, J. Q. Guo, *J. Electron. Mater.* **2014**, *43*, 2344.

[28] J. R. Salvador, J. Y. Cho, Z. Ye, J. E. Moczygemba, A. J. Thompson, J. W. Sharp, J. D. Koenig, R. Maloney, T. Thompson, J. Sakamoto, H. Wang, A. A. Wereszczak, *Phys. Chem. Chem. Phys.* **2014**, *16*, 12510.

[29] X. Hu, K. Nagase, P. Jood, M. Ohta, A. Yamamoto, *J. Electron. Mater.* **2015**, *44*, 1785.

[30] R. He, G. Schierning, K. Nielsch, *Adv. Mater. Technol.* **2018**, *3*, 1700256.

[31] G. Tan, M. Ohta, M. G. Kanatzidis, *Philos. Trans. R. Soc. A Math. Phys. Eng. Sci.* **2019**, *377*, 20180450.

[32] K. Bartholomé, B. Balke, D. Zuckermann, M. Köhne, M. Müller, K. Tarantik, J. König, *J. Electron. Mater.* **2014**, *43*, 1775.

[33] TEC TEG MFR , https://thermoelectric-generator.com/teg-cascade-800c-hot-side-thermoelectric-power-modules/ - Accessed: 17. September 2019.

[34] Novus Energy Technologies, http://www.novusenergytechnologies.com/technologies/power_generation.html Accessed: 17. September 2019.

[35] Kryotherm, http://kryothermtec.com/medium-temperature-generating-modules-mars-series.html - Accessed: 17. September 2019.

[36] G. Joshi, B. Poudel, *J. Electron. Mater.* **2016**, *45*, 6047.

[37] Q. Zhang, J. Liao, Y. Tang, M. Gu, C. Ming, P. Qiu, S. Bai, X. Shi, C. Uher, L. Chen, *Energy Environ. Sci.* **2017**, *10*, 956.

[38] X. Hu, P. Jood, M. Ohta, M. Kunii, K. Nagase, H. Nishiate, M. G. Kanatzidis, A. Yamamoto, *Energy Environ. Sci.* **2016**, *9*, 517.

[39] P. Jood, M. Ohta, A. Yamamoto, M. G. Kanatzidis, *Joule* **2018**, *2*, 1339.

[40] R. Chetty, K. Nagase, M. Aihara, P. Jood, H. Takazawa, M. Ohta, A. Yamamoto, *Appl. Energy* **2020**, *260*, 114443.

[41] H. Iwasaki, S. Yokoyama, T. Tsukui, M. Koyano, H. Hori, S. Sano, *Jpn. J. Appl. Phys.* **2003**, *42*, 3707.

[42] H. Wang, R. McCarty, J. R. Salvador, A. Yamamoto, J. König, *J. Electron. Mater.* **2014**, *43*, 2274.

[43] ASTM C177-19, *Standard Test Method for Steady-State Heat Flux Measurements and Thermal Transmission Properties by Means of the Guarded-Hot-Plate Apparatus, PA*; 2019.

[44] L. I. Anatychuk, M. V. Havrylyuk, *J. Electron. Mater.* **2011**, *40*, 1292.

[45] L. Rauscher, S. Fujimoto, H. T. Kaibe, S. Sano, *Meas. Sci. Technol.* **2005**, *16*, 1054.

[46] S. Kwon, Y. G. Kim, S. Lee, J. C. Kim, In *20th IMEKO World Congress 2012*; Busan, Republic of Korea, 2012.

[47] Knud Zabrocki, C. Goupil, H. Ouerdane, Y. Apertet, W. Seifert, M. Eckhard, In *Continuum Theory and Modeling of Thermoelectric Elements*; Goupil, C., Ed.; Wiley-VCH: Berlin, Germany, 2016; pp. 1–74.

[48] M. Ohta, P. Jood, M. Murata, C.-H. Lee, A. Yamamoto, H. Obara, *Adv. Energy Mater.* **2018**, *9*, 1801304.

[49] P. Ziolkowski, P. Blaschkewitz, E. Müller, *Measurement* **2021**, *167*, 108273.

[50] J. Blumm, A. Lindemann, B. Niedrig, In *Proc. of 17th European Conference on Thermophysical*

Properties; 2003; Vol. 35/36, pp. 621–626.

[51] BIPM, IEC, IFCC, ILAC, ISO, IUPAC, IUPAP, OML, Guide to the Expression of Uncertainties in Measurement. Joint Committee for Guides in Metrology 100:2008, GUM 1995 with minor corrections,.

[52] R. McCarty, R. Piper, *J. Electron. Mater.* **2015**, *44*, 1896.

[53] S. B. Mahajan, R. D. Pierce, R. J. Stevens, In *Volume 6A: Energy*; American Society of Mechanical Engineers, 2013.

[54] ISO/REMCO Committee on reference materials, ISO Guide 35:2017 Reference Materials—Guidance for characterization and assessment of homogeneity and stability (ISO, 2017).